



Excellent quality microchannels for rapid microdevice prototyping: direct CO₂ laser writing with efficient chemical postprocessing

Matheus J. T. Vargas^{1,2,3,4} · Michel Nieuwoudt^{1,4} · Rui Ming Yong^{4,5} · Frederique Vanholsbeeck^{4,5} · David E. Williams^{1,3} · M. Cather Simpson^{1,5}

Received: 3 May 2019 / Accepted: 5 October 2019 / Published online: 16 October 2019
© Springer-Verlag GmbH Germany, part of Springer Nature 2019

Abstract

Rapid, simple microchannel prototyping is critical for the development of modern microfluidic devices and platforms. Laser cutting (ablation) using a commercially available continuous wave (CW) CO₂ laser followed by thermal bonding is one of the most common approaches for prototyping in thermoplastics such as polymethyl methacrylate (PMMA). However, this technique suffers from poorly controlled channel quality, inconsistent results from solvent-based post-processing, and inconsistency of thermal bonding. We have overcome these challenges through a systematic study of channel ablation in PMMA using a CW CO₂ laser. A new solvent treatment approach results in clearly improved microchannel quality and processing consistency, with negligible residual solvent. Thermal bonding of the processed material showed fourfold increase in bonding strength with full retention of PMMA's favourable optical clarity. As proof of concept, a high-quality three-layered microfluidic prototype is fabricated with this new method and its performance demonstrated.

1 Introduction

The rapid pace in development of micro-total analysis systems (μTAS) has led to the rise in availability of point-of-care and point-of-site microfluidic diagnostic tools. These

devices are able to integrate and perform several different functions simultaneously, such as precise metering of reagents and samples, sample preparation, sorting and processing, and detection of biomarkers (Bhagat et al. 2010; Strohmeier et al. 2015; Tang et al. 2016). These microfluidic devices offer many advantages, including automation of analytical procedures, cost effectiveness, ease of use, repeatable accuracy and reduced processing time, making them perfect candidates to dominate the diagnostic test industry in the next decade (Wlodkovic and Darzynkiewicz 2011; Gomez 2013; Streets and Huang 2013; Sackmann et al. 2014). The main type of material used in these types of diagnostic μTAS devices is thermoplastics, largely due to their relatively low cost and ability to readily translate smoothly into industrial processes (Sackmann et al. 2014).

Several methods such as hot embossing, injection molding and micro-thermoforming that have been applied to microfluidic chip manufacture can be transferred to industry, as they allow for fast and inexpensive fabrication on an industrial scale (Boone et al. 2002; Attia et al. 2009; Focke et al. 2011). However, these methods become too expensive and time consuming when used for initial development and fast-prototyping of new designs of microfluidic circuits. The use of thermoplastics for research development in microfluidics is thus often avoided despite the overwhelming advantages in technology transfer (Aghvami et al. 2017). However,

Electronic supplementary material The online version of this article (<https://doi.org/10.1007/s10404-019-2291-1>) contains supplementary material, which is available to authorized users.

✉ Matheus J. T. Vargas
matheus.vargas@auckland.ac.nz

✉ David E. Williams
david.williams@auckland.ac.nz

✉ M. Cather Simpson
c.simpson@auckland.ac.nz

¹ School of Chemical Sciences, The University of Auckland, Auckland, New Zealand

² The Photon Factory, The University of Auckland, Auckland, New Zealand

³ MacDiarmid Institute for Advanced Materials and Nanotechnology, Wellington, New Zealand

⁴ The Dodd-Walls Centre for Photonic and Quantum Industries, Dunedin, New Zealand

⁵ Department of Physics, The University of Auckland, Auckland, New Zealand

direct laser writing on polymers can speed up the technological transfer of these devices from initial development to the final point-of-care products seen in clinical settings, thus is a good candidate for rapid prototyping in the initial research stage (Klank et al. 2002; Cheng et al. 2004; Malek 2006; Hong et al. 2010).

Several low-cost commercial continuous wave (CW) CO₂ laser engravers are commercially available (for example, Epilog[®], Gravograph[®], Mactron[®], Trotec[®], Universal[®] and Xenotech[®], among others) and do not require high levels of user training for efficient operation (Moreira Gabriel et al. 2014). These lasers are quite suitable for laser micromanufacturing in inexpensive thermoplastics. The use of such substrates allows for easy and direct technology transfer from research laboratories to industry which has a manufacturing and economical preference for these materials (Chin et al. 2012). In particular, poly(methyl methacrylate) (PMMA) has become one of the main polymers for production of μ TAS chips due to its high mechanical and chemical stability, excellent dielectric properties, optical transparency and low cost (Chen et al. 2008; Urech and Lippert 2010).

When CO₂ laser machining is applied to a polymer, photochemical and photo-thermal processes occur that result in thermal, thermo-oxidative or mechanical breakdown (Chen et al. 2008). The impinging gas or plasma jet vaporizes fragments of the macromolecules (down to oligomers) or causes breakaway of particles from the polymer and filler.

PMMA is well suited for CO₂ laser machining since it is possible to achieve 100% monomers as the by-products (Urech and Lippert 2010; Said-Galiev and Nikitin 1992). However, a number of quality issues can arise in direct writing of channels in PMMA using laser machining, particularly when using inexpensive CW CO₂ laser machines. The main problems contributing to poor quality microchannels are laser power instability and low translational resolution of the laser platform and mechanical backbone in these machines, besides mechanisms inherent in the laser ablation itself. Debris can be ejected the instant the laser ablates the material before re-melting can occur. Other problems are poor edge quality of the walls and borders (with formation of cracks) and poor smoothness of the channel walls. As such, the quality of the channels generated solely by laser machining is unsatisfactory for reliable prototyping. Several studies have attempted to optimize settings to improve CW CO₂ laser machining process but have used a modelling rather than an empirical approach, or lacked detailed consideration of reproducibility of the channels and fluid flow, or have limited the focus to the channel dimensions and not the quality (Klank et al. 2002; Nayak et al. 2008; Hong et al. 2010; Romoli et al. 2011; Kant et al. 2015; Prakash and Kumar 2015).

Thus, laser ablation of PMMA and other thermoplastics in isolation generates relatively poor quality channels, and it

is unfortunately unsatisfactory for reliable prototyping when used in the absence of post processing steps. A better understanding of the thermodynamics and the effect of different power settings and scan speeds could be used to generate effective post-treatment methods for improving the roughness and quality of the channels. To this end, we constructed an extensive database from empirical information, not just of the dimensions of the channels, but also on their quality regarding different aspects related to CO₂ laser machining.

PMMA is an amorphous polymer, hence it does not melt at a single, well-defined temperature, but instead softens at elevated temperatures, having a glass transition temperature (T_g) between 100 and 122 °C depending on grade or supplier (Zhu et al. 2007). Various studies have explored the T_g of PMMA to optimize the thermal bonding or have used temperature as a variable to improve the quality of the channels (Chen et al. 2003; Lin 2003; Nikcevic et al. 2007; Li et al. 2008; Ogończyk et al. 2010). The laser cutting process relies on effective use of the energy delivered as heat to allow the flow of the polymer and to decrease the roughness of the microchannel area on the polymer surface. In addition to a smooth microchannel, the transparency of polymer is important, especially around the detection area of microfluidic devices used in colorimetric, absorbance and fluorescence analytical applications (Gómez-de Pedro et al. 2017; Lefèvre et al. 2015).

The importance of creating smoother microchannels cannot be underestimated for the future of microfluidics and nanofluidics fields. The smoothness of microchannels has been shown to highly affect the shear viscosity and the hydrodynamic boundary slip during fluid flow (Asproulis and Drikakis 2011; Papanikolaou et al. 2016, 2017). Furthermore, models on the influence of the microchannel wall stiffness during fluid flow have shown to affect both the slip process and the thermal equilibrium at the solid–liquid interface (Asproulis and Drikakis 2010). Hence, different polymer stiffness and the roughness of the micro or nano-microchannel walls are important factors for a controlled fluid flow. These studies indicate that the use of channel smoothing techniques in stiff polymers that have an easier transition to industry, such as PMMA, can give rise to fast-prototyping nanofluidic chips using laser direct writing.

Whilst there is scope for optimization of the laser parameters, additional post-machining treatments are necessary to produce channels of quality suitable for prototyping. Solvent treatments show promise for post-ablation treatment. In contrast to thermal treatments, solvents act only on the surface of the polymer and therefore do not affect the bulk physical or chemical properties of the polymer. However, controlling the rate of evaporation and distribution of the solvents on the channels in both solvent vapour and liquid solvent treatments is challenging. Here we developed a reproducible solvent treatment enabling careful control of the solvent–polymer

dissolution, by total immersion of the polymer in a solvent bath at controlled temperature. This method delivers reproducible results because it does not depend on external factors such as distance from solvent vapour to the area to be treated, external temperature, or rate of evaporation.

In this paper we present an extensive database of CO₂ laser settings in terms of laser scan speed and power, with evaluation of the resulting microchannel quality and dimensions in PMMA. We additionally describe a novel chemical (solvent) surface treatment that both improves the quality of the channels and increases the bond strength of three-layer-based microfluidic chips, while keeping the detection area of the device transparent.

2 Materials and methods

2.1 Sample manufacturing

The substrates used for laser ablation were clear PMMA 2 mm thick sheets (PSP Ltd., Auckland, NZ). The laser system used was a CW CO₂ laser (Universal Laser Systems, VLS3.50, 30 W, 10.6 μm) with a lens working distance of 50.8 mm, generating a 127 μm spot size. These conditions were maintained throughout the experiment. Using this system, 20 mm straight lines were machined using variable power settings and scan speeds that ranged from 1.2 to 10.2 W (16 steps in total) and 20–175 mm/s (13 steps in total), resulting in a total of 208 different settings. Three samples were used for each setting. The overlap of fluences is presented in this experiment. 35 sets of fluence measurements (in duplicate) were made to study the effects of the speed and power. In addition, a set of square chambers with

surface area 10 mm² were machined using the raster mode of the laser system at 10.2 W and 175 mm/s to be used for chemical analysis. The microfluidic chips that were produced to verify channel quality and performance consisted of three different layers of 2 mm thick PMMA. The top layer contained the outlets, the second layer a detection window (chamber) and channels (Fig. 1c) and the third layer was the base layer. The laser power setting used for these was 7.8 W and the scan speed was 62.5 mm/s. The three layers were attached and sealed by thermal bonding under steel (5 mm) plates at 140 °C for 41 min and 2.2 MPa, then cooled to room temperature inside the steel plates.

2.2 Chemical treatment

For post-ablation chemical treatment, a boiling bath (82.3 °C) of isopropyl alcohol (EMPARTA[®] ACS, Merck) was used, with submersion of the samples for 75 s. By keeping the solvent at boiling temperature, we maintain a homogenous and reproducible solvent treatment without the need for high precision heating plates. The samples were left to quickly air dry and then heated at 90 °C for 12 h to remove the excess solvent.

2.3 Characterization and tests

The width of the channels, edge quality, bottom surface quality and start of the channel (Fig. 1a), were qualitatively characterized using a SEM (JCM-6000PLUS NeoScope Benchtop). A gold sputter coater (Quorum Technologies—Q150R) was used to create a conductive layer on the PMMA samples prior to SEM analysis.

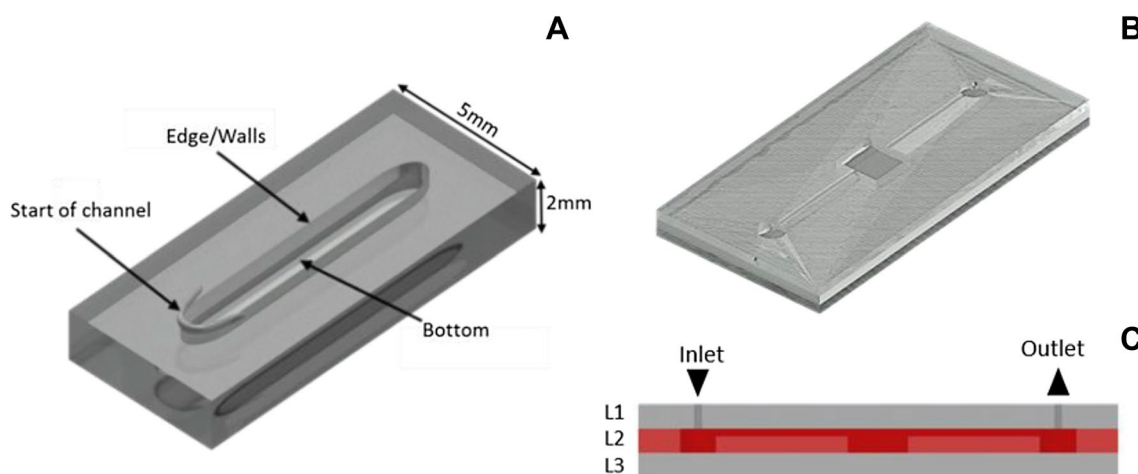


Fig. 1 **a** The four parameters measured: channel width, edge quality, bottom surface quality and start of the channel. **b** Proof-of-concept microfluidic test device with 80×40 mm, 10 mm² central optical window and input window of 3 mm radius. **c** Cross-section of the

proof-of-concept test device showing the three layers (L1, L2 and L3) and the channel, inlet and outlet layer and the base layer. The radius of the inlet and outlet ports are 0.6 mm radius and the red layers represent the machined and solvent treated surfaces

The depth and profiles of the channels were measured using a custom made spectral domain optical coherence tomography (SD-OCT) system to acquire two-dimensional cross-section of the sample. The system uses a broadband super-luminescent diode (SLD) (Superlum, Ireland), with a central wavelength of 840 nm, a bandwidth of 100 nm giving a theoretical depth resolution of 3.1 μm in air (Lippok et al. 2012). The signal-to-noise ratio of the system was approximately 95 dB. The lateral resolution was measured to be 21 μm . Only one sample for each parameter was imaged by OCT.

Fourier transform infrared spectroscopy (FTIR) spectra were recorded of the polymer surfaces in attenuated total reflectance (ATR) mode using a PerkinElmer Spectrum 400 FTIR spectrometer with KRS/diamond composite crystal window and single bounce at 45°, allowing interrogation of the surface to a depth of 4–6 μm , with averaging of eight scans at spectral resolution of 4 cm^{-1} . Spectra were recorded of both the machined chamber surfaces and adjacent surfaces to identify any changes in composition due to the laser machining, as well as any changes resulting from different treatments (untreated polymer, untreated polymer followed by treatment, ablated polymer, ablated polymer followed by treatment, and the evaporation of solvent residue by heating). The ethyl C–H deformation mode, $-\text{CH}_2$, of the polymer chains at 1435 cm^{-1} was used to normalize the spectra for comparison of the other vibrational bands for any changes resulting from the treatment.

A goniometer (KSV Instruments, CAM100) was used to measure the static contact angle and to calculate the surface energy of the treated and untreated samples. An Electroplus E3000 unit (Instron, High Wycombe, UK) was used to measure the bond strength of solvent treated and untreated PMMA bonded in a 600 mm^2 area.

The performance of the microfluidic chip constructed for proof-of-concept was tested using distilled water and blue food dye. Initially the channels in the microcircuit were filled using a syringe pump (Dolomite Mitos Syringe Pump XS) at 100 $\mu\text{l}/\text{min}$. A blue food dye was added to ultra-purified water and the pump rate was increased to 600 $\mu\text{l}/\text{min}$. The entering and mixing of the dye with the water in the detection chamber were analysed using an optical microscope (Leica, DF450C-M205FA components).

The surface roughness of the treated and untreated PMMA was analysed using optical profilometry (Contour GT-K, Bruker USA). Finally, the transparency of the detection windows of the solvent-treated and untreated microfluidic chips was analysed using a UV–Vis spectrophotometer (Ocean Optics S2000-UV–Vis) and a rhodamine B (Sigma-Aldrich) 8.35 μM solution in ultra-purified water.

3 Results and discussion

3.1 Channel dimensions

The dimensions resulting from the different settings of the variables were correlated with scan speed and power of the laser, which can also be translated into fluence. The relationship between channel width and variations in speed and power is given in Fig. 2a, b. Speeds above 180 mm/s and below 20 mm/s resulted in very poor quality channels that did not allow for proper measurements. The channel width increases logarithmically with power, as we increase the laser power while keeping the speed constant. This is consistent with what we expect from the Gaussian profile of the commercial CO_2 lasers and with previous reports in the literature (Snakenborg et al. 2004; Chung et al. 2005). The width of the channels varied from 58 to 264 μm , depending on laser power and at different speed settings, with standard deviation (SD) between 3 and 22 μm and an average of 11 μm . The variation in SD for the channel width measured using the SEM is mostly due to variation in location where channels were measured and imperfections in some of the channels due to errors in the laser oscillation. However, the standard deviations using speeds around 80–100 mm/s at powers between 10 and 6 W were lower, with lowest standard deviations for lower powers between 1.8 and 3 W at scanning speeds of 40–100 mm/s .

The depths of the channels measured using OCT varied from 14 to 1360 μm . The channel depth measurements were affected similarly to the SEM measurements.

The scan speed and laser power were varied while keeping the fluences the same, to determine the effect of these parameters on the quality of the channels. The correlation between the fluence (calculated using scan speed and laser power) and width and depth of the channels is displayed in Fig. 2c. It was found that lower scan speed and laser power are correlated with lower standard deviations ($p < 0.05$) at fluence below 13 J/cm^2 in contrast with using higher scan speed and higher laser power to achieve the same fluence. At higher fluences, there was no correlation between standard deviation and scan speed and laser power. This result indicates that lowering both laser power and scan speeds allow greater reproducibility in channel dimensions.

The fitted depth profiles of the channels measured by SD-OCT are shown in Fig. 2d for five different fluences. A Gaussian profile for the channel can be identified, as expected from the CO_2 laser beam profile. After the solvent treatment there was no significant difference in the measurements of width and depth as the treated sample values were within the standard deviation.

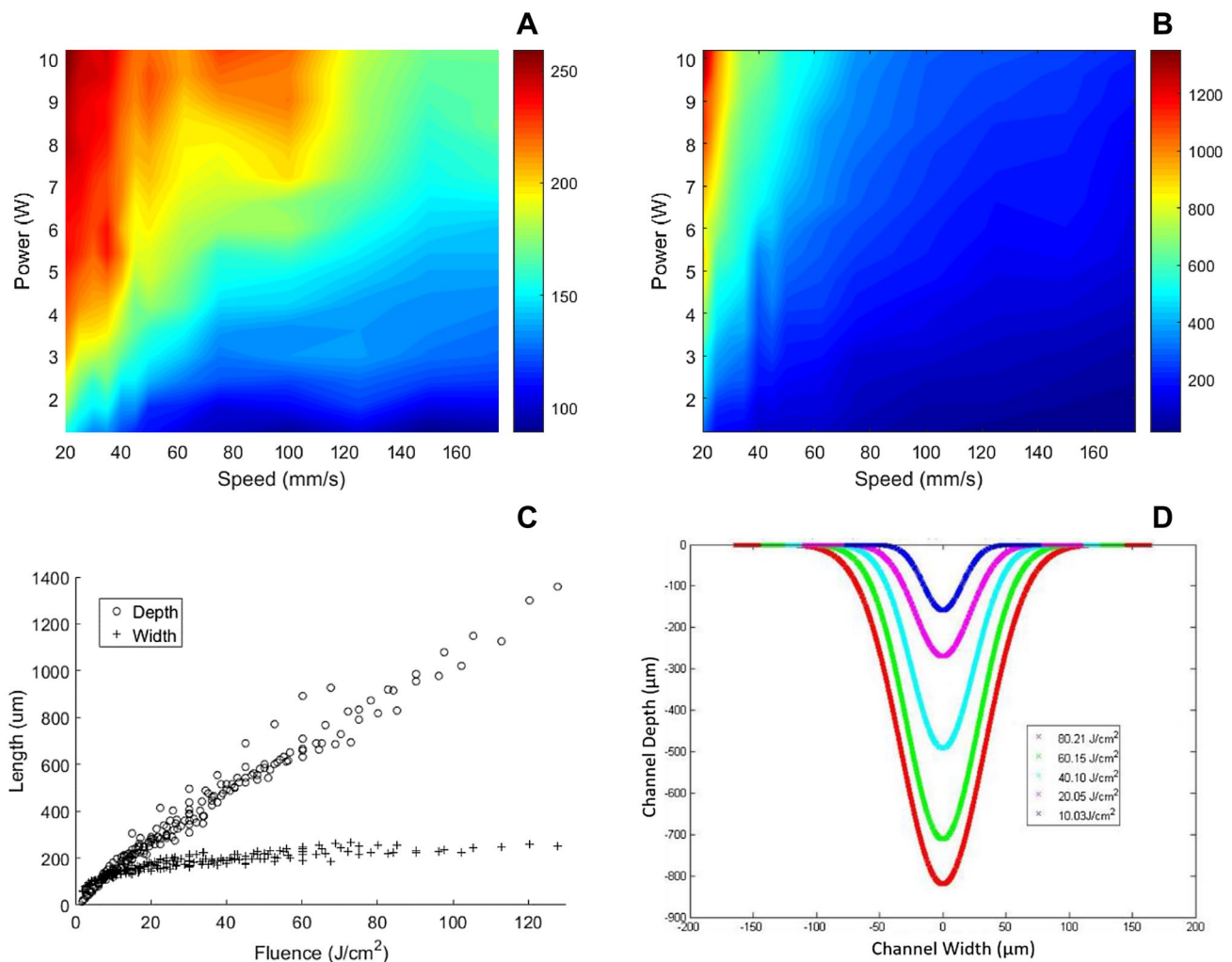


Fig. 2 **a** Channel width/ μm as measured by SEM and **b** depth/ μm (right) as measured by OCT as a function of laser power and scan speed as contour plots. **c** Width (crosses) and depth (open circles) of

channels as a function of incident laser fluence. **d** Channel profiles fit from data acquired by OCT

3.2 Qualitative analysis

SEM is a useful tool to compare morphologies of samples (Golding et al. 2016). Here we used the SEM images of the channels to assess and compare the quality of channels over the whole range of powers, scanning speeds and treatments used. This analysis of the samples confirmed the need to optimize these settings to avoid formation of inferior quality channels. Channel quality was graded qualitatively based on the observations of morphology, on a scale from 0.5 to 5, with 5 denoting the highest quality and 0.5 the lowest. The parameters assessed were edge/wall quality, bottom quality and shape of the start of the channel. Figure 3 shows the relationships between these parameters in the untreated samples. The bottom quality was improved at lower scan speeds between 20 and 40 mm/s and lower laser powers between 4.2 and 7.8 W (fluence 10.52 and 39.10 mJ/cm²). The edge/wall

quality in these samples followed a similar trend (Supplementary information), but it was also improved using high scan speeds and high laser powers, between 40–60 mm/s and 8–10.2 W (13.03–25.57 mJ/cm²), respectively. The graphical results for the quality parameters of the edges and start of channel are given in the Supplementary information.

It is important to notice that in this section, we are dealing with qualitative or categorical results. These results were generated by the evaluation of multiple samples and different researchers classifying the data in the experiment according to a set scale. To verify the uncertainty related to the visual quality classification, we have created ordinal variables (0.5 is “poor” and 5 is “very good”), used 0.5 units steps when evaluating the channel and averaged the sample values to a final quality classification. During the experiment, the standard deviation between the qualitative classification of the same sample was approximately ± 0.25 units of the qualitative scale,

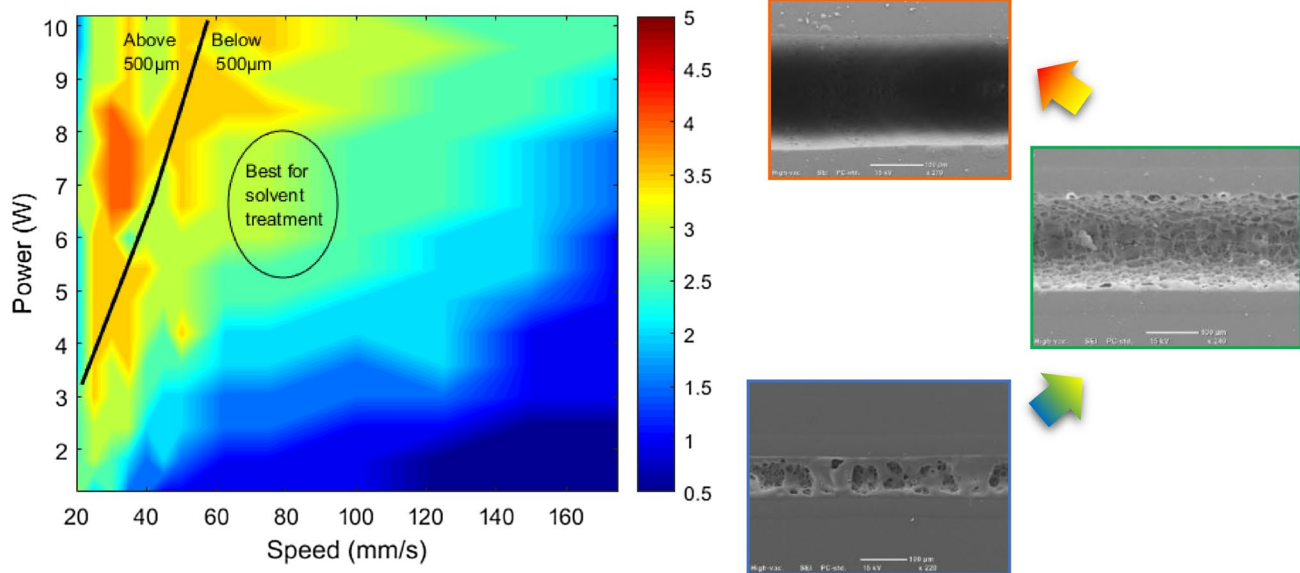


Fig. 3 (Left) Qualitative colour map of the quality of the untreated bottom (control) of the channels (colour scale on right: 0.5–5, lowest to highest quality). The images on the right illustrate ‘poor’ (quality value 0.5), ‘medium’ (quality value 3) and ‘good’ (quality value

5) channels. The map shows that the areas where the solvent is most effective are where the channels are not too deep, allowing for solvent treatment (colour figure online)

which represented a coefficient of variation of 9.5% for the analysis of the bottom of the channels, 8.1% for the debris at the end of the channels and 10.2% for the edge of the channels.

Solvent treatment was performed to smooth the channels and remove the debris using Isopropyl alcohol at its boiling point. A solvent is most effective when the forces of attraction between the solvent molecules are smaller than the forces of attraction between the polymer and solvent (Brydson and Ebrary 1999), and can be characterized by the Hildebrand solubility parameter (δ), which describes the enthalpy of mixing (Kwei 1992). Polymers dissolve in solvents for which the solubility parameter is similar (Miller-Chou and Koenig 2003) and for which the Gibbs free energy on mixing is below zero (Hansen 2000). The Gibbs free energy on mixing (ΔG_m) during the dissolution of an amorphous polymer in a solvent is given by:

$$0 > \Delta G_m = \Delta H_m - T\Delta S_m, \quad (1)$$

where (ΔH_m) is the enthalpy change on mixing, (T) is temperature and (ΔS_m) is the entropy change on mixing. The dissolution of high molecular weight polymers is associated with a small positive entropy change. The Hildebrand parameter also provides a measure of the cohesive molecular forces of each of the solvent and solute. The energy required to break the intermolecular physical links in a unit volume of a material, cohesive energy density (CED), can be related to the solubility parameter as follows:

$$\delta = (\text{CED})^{1/2} = \left(\frac{\Delta H_{\text{vap}} - RT}{V} \right)^{1/2}, \quad (2)$$

where ΔH_{vap} is the enthalpy of vaporization, (R) is the gas constant, and (V) is the molar volume of the solvent. Several studies have demonstrated the use of different solvents to bond PMMA (Ogilvie et al. 2010; Steigert et al. 2007; Tsao and DeVoe 2009), but these did not explore the effect of such treatments on the quality of the channels nor on the effect on the bond strength between the PMMA layers in the microfluidic device.

The solubility parameter of PMMA is 20.18 MPa^{1/2}, and solvents such as dichloromethane, acetone and isopropyl alcohol and water are, respectively, 20.1 MPa^{1/2}, 19.9 MPa^{1/2} and 23.4 MPa^{1/2} and 47.9 MPa^{1/2} at room temperature (Tsao and DeVoe 2009; Ng et al. 2008) PMMA is not affected by water or by isopropyl alcohol at room temperature, but is attacked by dichloromethane and acetone. Therefore, using solvents with similar solubility parameters would only work when using a solvent vapour to smooth and clean the channels. The solubility parameter can be manipulated by changing the temperature as seen in Eq. (2). If we increase the temperature of isopropanol we can decrease the solubility parameter to bring its value closer to that of PMMA. Table 1 shows the change in solubility parameter as we change the temperature and therefore the enthalpy of vaporization.

This solvent treatment demonstrates a significant increase in the overall quality of the channels and a visible decrease or complete removal of debris from inside of the channels (Fig. 4) as well as debris located at the end of the machined lines (Fig. 5).

Table 1 Solubility parameter for isopropanol and the constants used in its calculation (Majer et al. 1985; Haynes 2012)

Environment	Solubility parameter (MPa ^{1/2})	Temperature (K)	Enthalpy of vaporization (kJ/mol)	Molar volume (m ³ /mol)
Room temperature	23.7	298.15	45.39	7.65E-05
Boiling point	21.8	355.5	39.85	7.65E-05

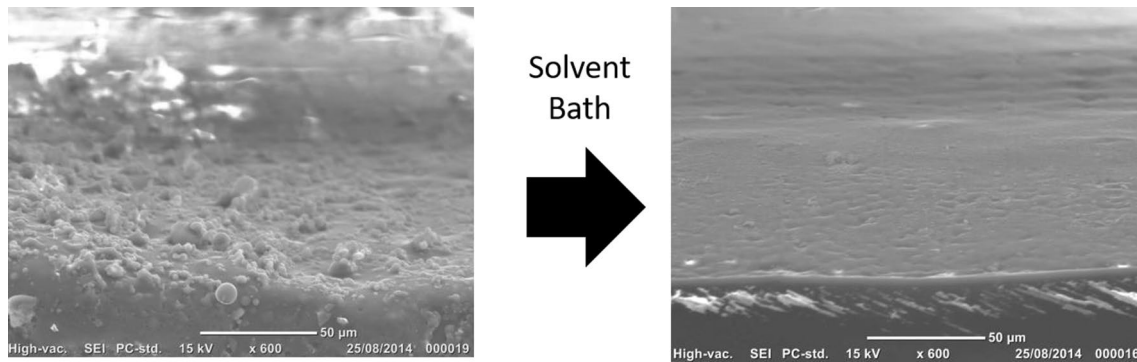


Fig. 4 (Left) Channel floor surface after direct laser writing. (Right) Decrease or removal of debris from inside the microchannel after solvent treatment

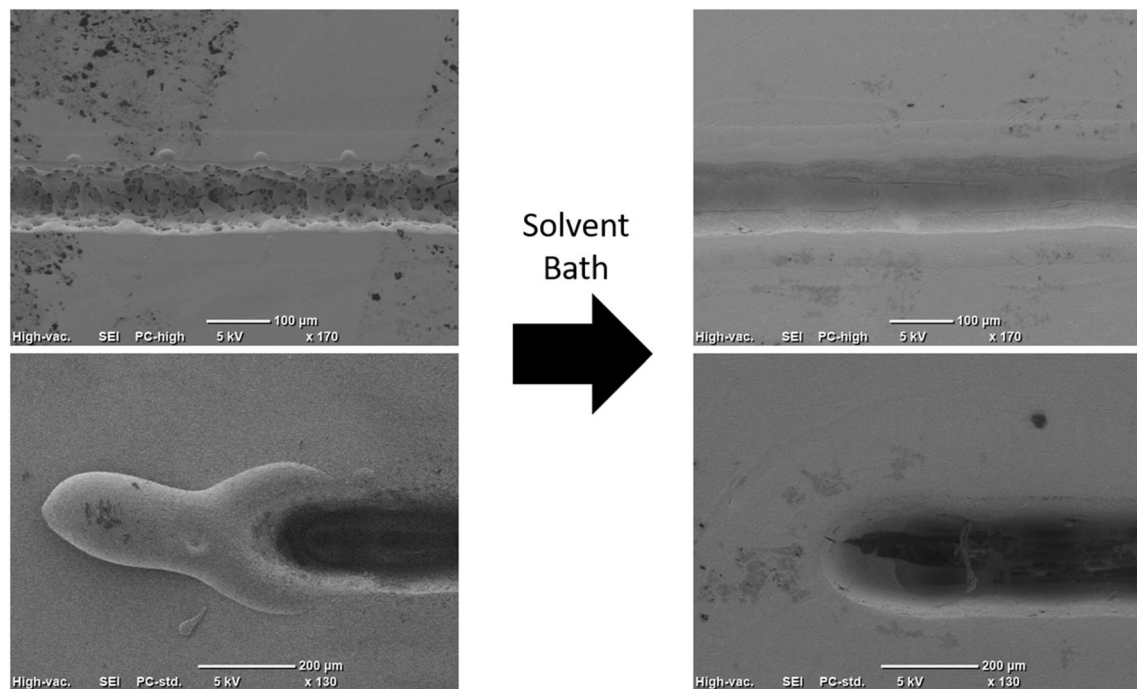


Fig. 5 Debris at the edges and at the end of the line being removed by the solvent bath technique

The qualitatively assessed quality parameters for the edge and bottom of the channels following the solvent treatment follow a similar trend to the untreated, control sample related to which settings give the best outcomes (Supplementary information). The surface quality of the channel

floors created using lower fluences is greatly increased after boiling isopropyl submersion. For surfaces made using higher fluences, improvement is either slight or none, even worsened. This is due to difficulties for the solvent to reach the bottom of the channels (Fig. 6). The dimensions of the

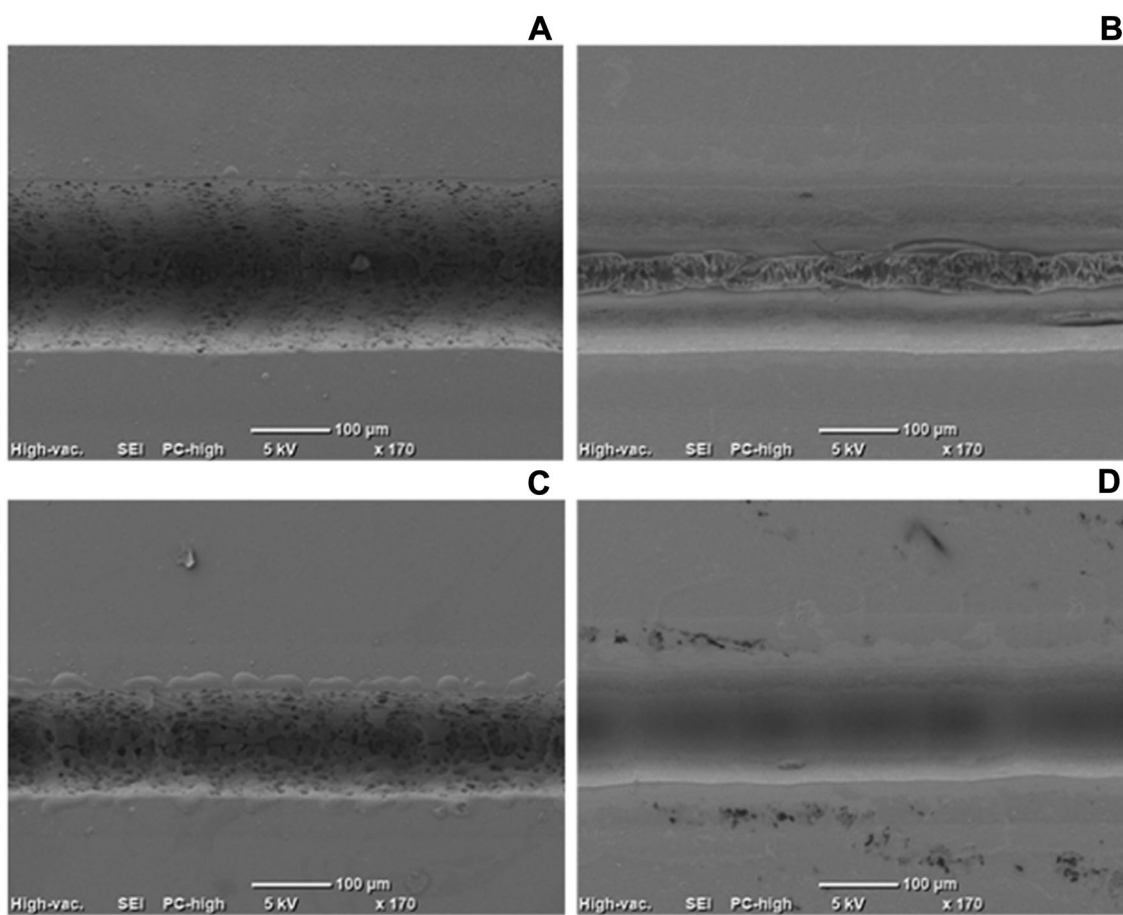


Fig. 6 Deeper channels before (top/left) and after (top/right) solvent treatment showing unaffected interior dimensions (parameters: 30 mm/s, 9.6 W, 80.20 mJ/cm², 819 μm deep). The untreated channel

(bottom/left) and solvent smoothed (bottom/right) shallow channel (parameters: 30 mm/s, 4.2 W, 35.09 mJ/cm², 478 μm deep)

channels treated with boiling isopropanol were within the standard deviation found in the control samples, showing that our treatment process did not significantly affect the microchannel dimensions. However, as the solvent treatment is still an etching technique care must be taken to not immerse the samples for too long, even for deeper channels, placing a limitation on the immersion time.

Another change in morphology resulting from the solvent treatment and not previously reported, were steps or grooves created in the channel as the laser raster scans the surface (Fig. 7). A possible cause for this is an intrinsic property of the laser equipment that originates from small, rapid power oscillations from the stepper motor belt that moves the laser head. These step defects can be improved using scan speeds below 100 mm/s and laser power below 6 W (up to 15.03 mJ/cm²). Lower scanning speeds and laser powers result in poorer quality or even unformed channels (Supplementary information). Furthermore, Fig. 3 shows an optimal range for the machining parameters for which post-treatment of the channels was effective in retaining a good quality.

3.3 Surface chemistry analysis

An important consideration in microfabrication incorporating chemical treatment is characterization of any chemical changes on the polymer surface or chemical residues that may be present post-treatment. PMMA surfaces from two treatments were compared with those of the control; the first was the laser machining and the second was solvent treatment of the laser machined area with the boiling isopropyl alcohol procedure described earlier. FTIR spectra of the plain PMMA surface (green), laser machined surface (red) and laser machined surface followed by solvent treatment (black) are given in Fig. 8. All spectra were peak height normalized to the ethyl C–H deformation mode at 1451 cm⁻¹ and overlaid for comparison, with an inset showing an expanded view of the fingerprint region. The decrease in intensity of the strong bands at 1723 cm⁻¹ (C=O stretch mode) and 1188 and 1143 cm⁻¹ (C–O–C stretching modes) after laser ablation (red spectrum) clearly shows that laser ablation reduces the relative amount of carbonyl groups on the PMMA surface.

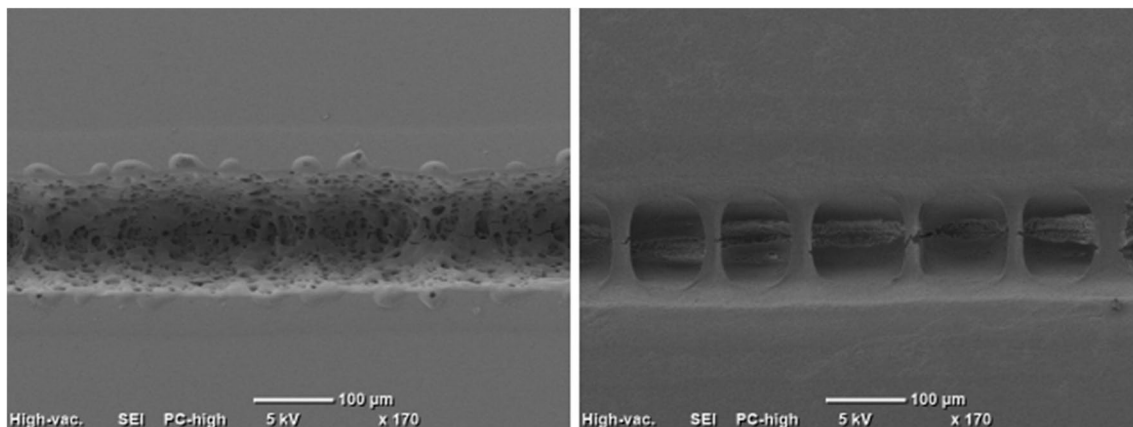
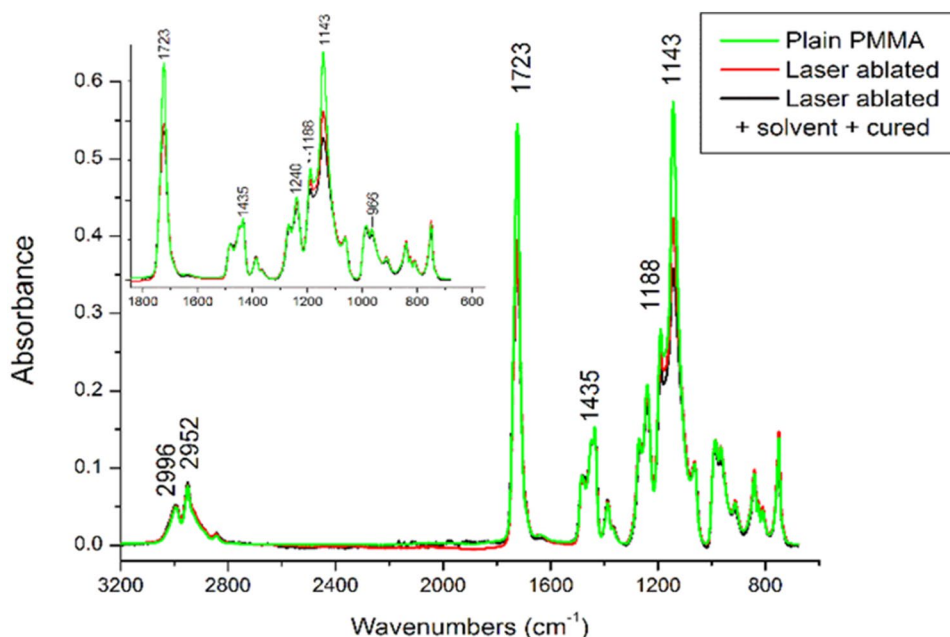


Fig. 7 Periodicity found in channels (parameter shown: 60 mm/s, 9 W, 15.03 mJ/cm³) and evident through the solvent treatment method. (Left) Untreated and (right) treated sample

Fig. 8 ATR FTIR spectra of untreated PMMA surfaces (green), after laser ablating (red) and after treatment with IPA followed by curing (black). Inset shows expanded view of the reduction in C–O (1143 and 1186 cm⁻¹) and C=O bonds (1723 cm⁻¹) (colour figure online)



The results confirm the observation by Klank et al. (2002) and Nayak et al. (2008) of thermal degradation of the surface by the laser. Other studies on the decomposition of PMMA using 10.6 μm lasers demonstrate that the full degradation pathway due to laser-induced heating can result in (up to 100%) formation of methyl methacrylate (MMA) monomers (Srinivasan 1993). In addition, generation of CO and CO₂ can occur and is likely responsible for the observed decrease in relative amounts of C=O and C–O–C. The use of boiling isopropyl alcohol resulted in adsorption of the solvent on the polymer surface in both the ablated and non-ablated part of the polymer: solvent residue was detected on all the treated samples and was removed only by curing them at 90 °C for 12 h, which is above the boiling point of isopropyl alcohol but well below the transition glass temperature of PMMA.

Figure 9 shows the decrease in the C–O band at 952.5 cm⁻¹ as the isopropyl alcohol was eliminated after the heat treatment.

After the solvent treatment was applied to the machined area, further, but smaller, decreases in the relative intensities of the C–O–C and C=O modes were observed. These changes suggest that the boiling solvent treatment was also working as a means to wash off by-products of PMMA monomers resulting from the laser machining. In addition, the byproduct dissolved in the isopropyl alcohol wash was analysed and found to comprise largely acrylic groups.

An additional comparison of the surface for any differences resulting from pre- and post-treatment was performed by measuring the contact angle of each surface. The untreated and treated polymers showed contact angles of 70.8° ± 1.7° and 71.0° ± 2.0°, respectively. These results

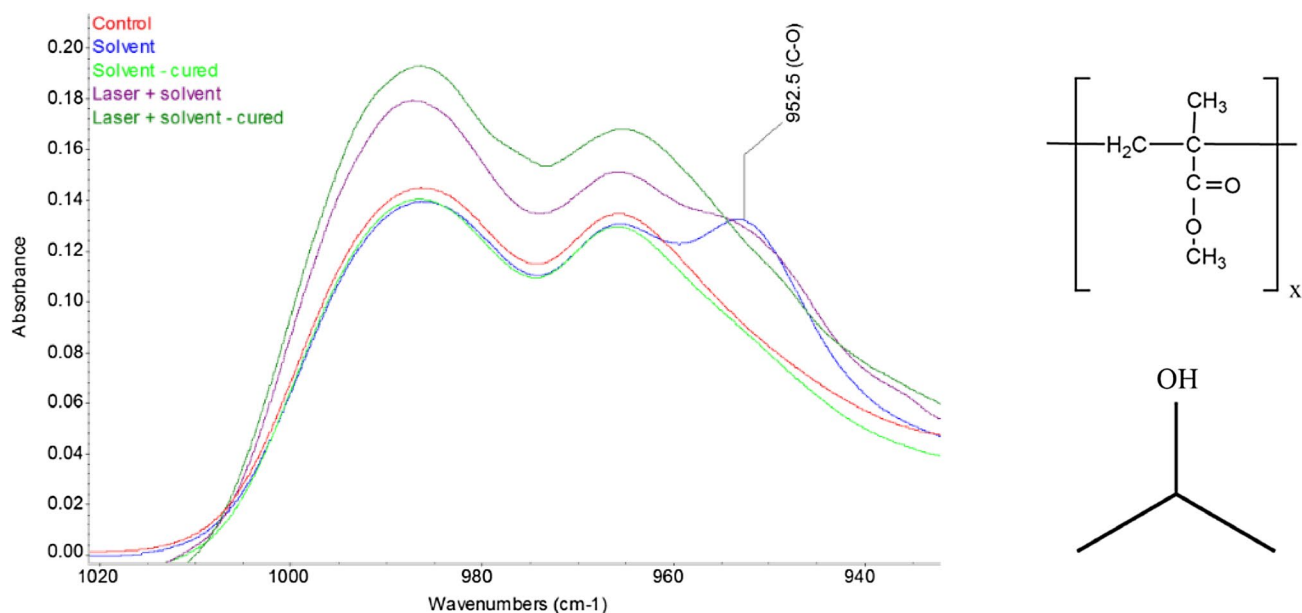


Fig. 9 FTIR spectra of the C–O stretch mode of IPA at 950 cm^{-1} during solvent treatment: control (red), solvent applied to control (PMMA sheet) (blue), solvent applied to control followed by temper-

ature curing (light green), solvent on the laser ablated PMMA (purple) and solvent treatment on the laser ablated surface followed by temperature curing (dark green) (colour figure online)

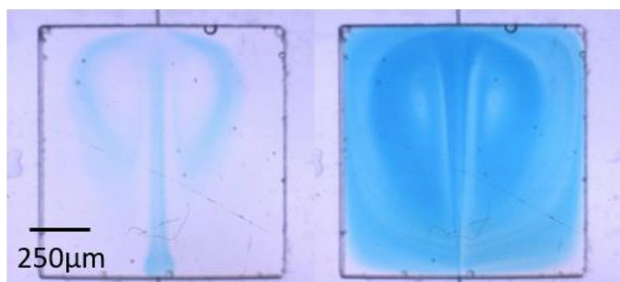


Fig. 10 Visible detection window created with the presented method. Images taken (left) after 5 s and (right) after 60 s of blue food dye as it began to enter the microfluidic chamber (colour figure online)

indicated that no significant changes were likely to occur in the polymer wettability when using this technique for microfabrication.

3.4 Proof-of-concept: a microfluidic device

Microfluidic devices often incorporate an analytical tool or sensor on at least one segment of the microfluidic circuit. Some detection is performed using spectral, fluorometric or colorimetric measurements. These techniques have in common the requirement of a clear and reproducible optical detection window. One of the effects of the solvent treatment is a slight cloudiness on the surface of the polymer due to adsorption of acrylic particles from the solution as well as increase in surface roughness (see next section); these affect the transparency. In this study, we used thermal bonding

after solvent treatment of the channels to create a microfluidic chip setup that allow us to keep the transparency of the detection chamber, while achieving smoothing of the channel surfaces as previously described. Mixing of water and blue dye solution and vortex formation inside the detection chamber could clearly be observed in the microfluidic chamber through the transparent optical window (Fig. 10). When using colorimetric analysis in microfluidics as well as verifying the turbulence, mixing, and miscibility of

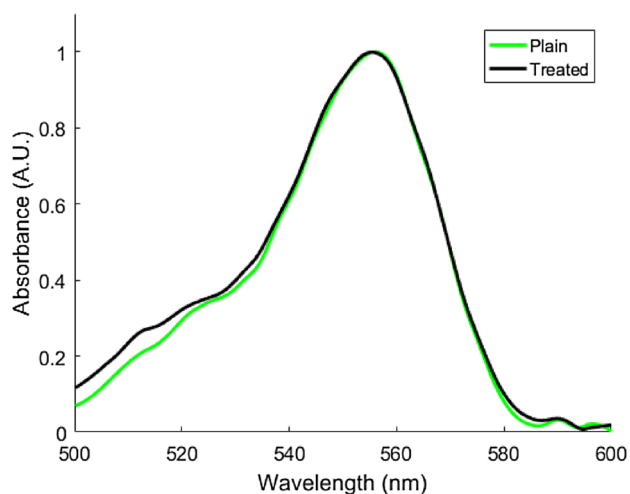


Fig. 11 Main rhodamine B peak at 556 nm showing highly similar absorbance peak for treated and untreated samples, hence the effectiveness of using a three-layer sandwich chip when using the solvent treatment

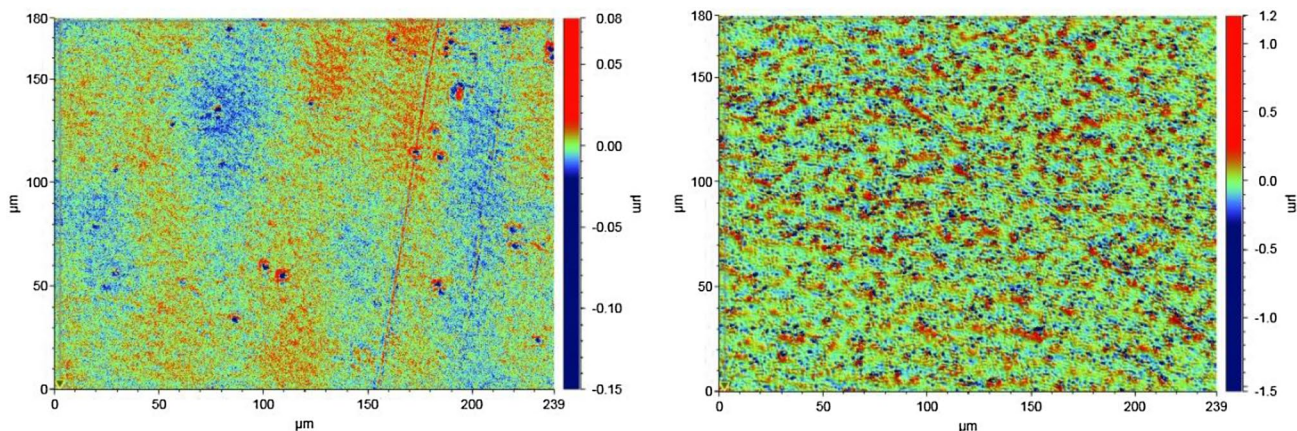


Fig. 12 Surface profile acquired using an optical profilometer (colour scale/ μm) of the same area analysed before and after solvent treatment. Left: untreated PMMA showing some depressions (blue) that

may trap air. Right: increase in surface roughness seen after treatment (colour figure online)

fluids, transparency of the detection window transparency is critical.

PMMA absorbs strongly in the UV region, therefore rhodamine B was used to test the transparency of the detection window as it absorbs strongly at the visible region. The similarity of absorbance intensity for treated and untreated samples showed that no effective change in absorption occurred (Fig. 11).

The bonding technique in microfluidic prototypes needs to be inexpensive, easy and fast. Thermal bonding fulfils these requirements. The strength of thermal bonding in our system was tested by bonding a treated area with an untreated area to simulate the bond between the smoothed channel surface and optically transparent PMMA. The bond strength of the untreated PMMA was 185.0 ± 33.3 kPa (111 N per 600 mm^{-2}), and 808.0 ± 80 kPa (545 N per 600 mm^{-2}) for the thermally bonded treated and untreated samples.

The increase in strength for the treated polymer bonding is likely due to slight swelling of the polymer, which creates a micro roughness (Fig. 12). The optical profile results also showed some air traps that were not seen in treated samples. The extra roughness on the surface generated by the solvent treatment allowed air to be released from the trapped areas during the thermal bonding process and so increase the contact area. Consequently, the bond strength was increased.

To calculate and compare the surface roughness of the samples we used the standard measurement for roughness parameters of arithmetical mean roughness value (R_a) and the root-mean-square of the roughness (R_q) (Petropoulos et al. 2010). The R_a and R_q found for the untreated sample were, respectively, 6 and 7 nm, whereas for the treated samples these values increased to 81 and 115 nm. We credit this roughness difference to increasing the effective bonding area by decreasing the air bubbles trapped,

and by increasing the effective bonding depth when the treated sample is used.

4 Conclusion

We have developed a protocol for making microfluidic circuits using a rapid prototyping technique while still achieving good quality channels. This protocol utilizes variation in laser power and scan speeds to generate different microchannels dimensions. The use of boiling isopropanol is a rapid means to reproducibly smooth the rough microchannels and debris that result when using commercially available CO_2 lasers, and can be applied and removed from the sample surfaces without altering their properties. A proof-of-concept microfluidic chip confirmed that we could retain the optical transparency of the detection window, while an approximately fourfold increase was achieved in the bonding strength for binding between an untreated and a treated sample. This protocol enables rapid prototyping of new microfluidic designs without the need for expensive equipment, providing greater opportunities for laboratories with limited resources.

Acknowledgements We acknowledge the New Zealand Ministry of Business, Innovation and Employment (UOAX1202) and Auckland UniServices for funding support. We also thank Orbis Diagnostics for the Ph.D. Fellowship funding to M. J. T. V.

References

- Aghvami SA, Opathalage A, Zhang ZK et al (2017) Rapid prototyping of cyclic olefin copolymer (COC) microfluidic devices. *Sens Actuators B Chem* 247:940–949. <https://doi.org/10.1016/j.snb.2017.03.023>

- Asproulis N, Drikakis D (2010) Boundary slip dependency on surface stiffness. *Phys Rev E Stat Nonlinear Soft Matter Phys.* <https://doi.org/10.1103/PhysRevE.81.061503>
- Asproulis N, Drikakis D (2011) Wall-mass effects on hydrodynamic boundary slip. *Phys Rev E* 84:31504. <https://doi.org/10.1103/PhysRevE.84.031504>
- Attia UM, Marson S, Alcock JR (2009) Micro-injection moulding of polymer microfluidic devices. *Microfluid Nanofluidics* 7:1–28
- Bhagat AAS, Bow H, Hou HW et al (2010) Microfluidics for cell separation. *Med Biol Eng Comput* 48:999–1014
- Boone TD, Fan ZH, Hooper HH et al (2002) Plastic advances microfluidic devices. *Anal Chem* 74:78A–86A. <https://doi.org/10.1021/ac021943c>
- Brydson J, Ebrary Inc (1999) *Plastics materials*, 7th edn. Butterworth-Heinemann, Oxford, Boston
- Chen Z, Gao Y, Su R et al (2003) Fabrication and characterization of poly(methyl methacrylate) microchannels by in situ polymerization with a novel metal template. *Electrophoresis* 24:3246–3252. <https://doi.org/10.1002/elps.200305534>
- Chen Y, Zhang L, Chen G (2008) Fabrication, modification, and application of poly(methyl methacrylate) microfluidic chips. *Electrophoresis* 29:1801–1814
- Cheng JY, Wei CW, Hsu KH, Young TH (2004) Direct-write laser micromachining and universal surface modification of PMMA for device development. *Sens Actuators B Chem* 99:186–196. <https://doi.org/10.1016/j.snb.2003.10.022>
- Chin CD, Linder V, Sia SK (2012) Commercialization of microfluidic point-of-care diagnostic devices. *Lab Chip* 12:2118. <https://doi.org/10.1039/c2lc21204h>
- Chung CK, Lin YC, Huang GR (2005) Bulge formation and improvement of the polymer in CO₂ laser micromachining. *J Micromech Microeng* 15:1878–1884. <https://doi.org/10.1088/0960-1317/15/10/013>
- Focke M, Kosse D, Al-Bamerni D et al (2011) Microthermoforming of microfluidic substrates by soft lithography (μ TSL): optimization using design of experiments. *J Micromech Microeng* 21:115002. <https://doi.org/10.1088/0960-1317/21/11/115002>
- Gabriel EFM, Coltro WKT, Garcia CD (2014) Fast and versatile fabrication of PMMA microchip electrophoretic devices by laser engraving. *Electrophoresis* 35:2325–2332. <https://doi.org/10.1002/elps.201470140>
- Golding CG, Lamboo LL, Beniac DR, Booth TF (2016) The scanning electron microscope in microbiology and diagnosis of infectious disease. *Sci Rep* 6:26516. <https://doi.org/10.1038/srep26516>
- Gomez FA (2013) The future of microfluidic point-of-care diagnostic devices. *Bioanalysis* 5:1–3. <https://doi.org/10.4155/bio.12.307>
- Gómez-de Pedro S, Berenguel-Alonso M, Couceiro P et al (2017) Automatic microfluidic system to perform multi-step magnetobiochemical assays. *Sens Actuators B Chem* 245:477–483. <https://doi.org/10.1016/j.snb.2017.01.158>
- Hansen CM (ed) (2000) *Solubility parameters—an introduction*. In: Hansen solubility parameters: a user's handbook. CRC Press, Boca Raton, FL, USA, pp 1–24
- Haynes WM (2012) *CRC handbook of chemistry and physics*, 93rd edn
- Hong TF, Ju WJ, Wu MC et al (2010) Rapid prototyping of PMMA microfluidic chips utilizing a CO₂ laser. *Microfluid Nanofluidics* 9:1125–1133. <https://doi.org/10.1007/s10404-010-0633-0>
- Kant R, Gupta A, Bhattacharya S (2015) Studies on CO₂ laser micromachining on PMMA to fabricate micro channel for microfluidic applications. In: Joshi NS, Dixit SU (eds) *Lasers based manufacturing: 5th international and 26th all india manufacturing technology, design and research conference, AIMTDR 2014*. Springer India, New Delhi, pp 221–238
- Klank H, Kutter JP, Geschke O (2002) CO₂-laser micromachining and back-end processing for rapid production of PMMA-based microfluidic systems. *Lab Chip* 2:242–246. <https://doi.org/10.1039/b206409j>
- Kwei TK (1992) *CRC handbook of polymer-liquid interaction parameters and solubility parameters* by Allan F M Barton, CRC Press (1990), ISBN 0-8493-3544-2, hard cover, 771 pp., price not available. *Polym Adv Technol* 3:47. <https://doi.org/10.1002/pat.1992.220030107>
- Lefèvre F, Juneau P, Izquierdo R (2015) Integration of fluorescence sensors using organic optoelectronic components for microfluidic platform. *Sens Actuators B Chem* 221:1314–1320. <https://doi.org/10.1016/j.snb.2015.07.077>
- Li SW, Xu JH, Wang YJ et al (2008) Low-temperature bonding of poly-(methyl methacrylate) microfluidic devices under an ultrasonic field. *J Micromech Microeng* 19:015035. <https://doi.org/10.1088/0960-1317/19/1/015035>
- Lin L (2003) Thermal challenges in MEMS applications: phase change phenomena and thermal bonding processes. *Microelectron J* 35(3):179–185
- Lippok N, Coen S, Nielsen P, Vanholsbeek F (2012) Dispersion compensation in Fourier domain optical coherence tomography using the fractional Fourier transform. *Opt Express* 20:23398. <https://doi.org/10.1364/OE.20.023398>
- Majer V, Svoboda V, Kehiaian HV (1985) *Enthalpies of vaporization of organic compounds: a critical review and data compilation*. Blackwell Scientific, Oxford
- Malek CGK (2006) *Laser processing for bio-microfluidics applications (part II)*. *Anal Bioanal Chem* 385:1362–1369
- Miller-Chou BA, Koenig JL (2003) A review of polymer dissolution. *Prog Polym Sci* 28:1223–1270
- Nayak NC, Lam YC, Yue CY, Sinha AT (2008) CO₂-laser micromachining of PMMA: the effect of polymer molecular weight. *J Micromech Microeng* 18:095020. <https://doi.org/10.1088/0960-1317/18/9/095020>
- Ng SH, Tjeung RT, Wang ZF et al (2008) Thermally activated solvent bonding of polymers. *Microsyst Technol* 14:753–759. <https://doi.org/10.1007/s00542-007-0459-1>
- Nikcevic I, Lee SH, Piruska A et al (2007) Characterization and performance of injection molded poly(methylmethacrylate) microchips for capillary electrophoresis. *J Chromatogr A* 1154:444–453. <https://doi.org/10.1016/j.chroma.2007.03.125>
- Ogilvie IRG, Sieben VJ, Floquet CFA et al (2010) Solvent processing of PMMA and COC chips for bonding devices with optical quality surfaces. In: *14th international conference on miniaturized systems for chemistry and life sciences*, pp 1244–1246. <https://doi.org/10.1088/0960-1317/20/6/065016>
- Ogończyk D, Wegrzyn J, Jankowski P et al (2010) Bonding of microfluidic devices fabricated in polycarbonate. *Lab Chip* 10:1324–1327. <https://doi.org/10.1039/b924439e>
- Papanikolaou M, Frank M, Drikakis D (2016) Nanoflow over a fractal surface. *Phys Fluids*. <https://doi.org/10.1063/1.4958975>
- Papanikolaou M, Frank M, Drikakis D (2017) Effects of surface roughness on shear viscosity. *Phys Rev E* 95:33108. <https://doi.org/10.1103/PhysRevE.95.033108>
- Petropoulos GP, Pandazaras CN, Davim JP (2010) Surface texture characterization and evaluation related to machining. In: Davim JP (ed) *Surface integrity in machining*. Springer, London, pp 37–66
- Prakash S, Kumar S (2015) Fabrication of microchannels on transparent PMMA using CO₂ laser (10.6 μ m) for microfluidic applications: an experimental investigation. *Int J Precis Eng Manuf* 16:361–366. <https://doi.org/10.1007/s12541-015-0047-8>
- Romoli L, Tantussi G, Dini G (2011) Experimental approach to the laser machining of PMMA substrates for the fabrication of microfluidic devices. *Opt Lasers Eng* 49:419–427. <https://doi.org/10.1016/j.optlaseng.2010.11.013>
- Sackmann EK, Fulton AL, Beebe DJ (2014) The present and future role of microfluidics in biomedical research. *Nature* 507:181–189. <https://doi.org/10.1038/nature13118>

- Said-Galiev ÉE, Nikitin LN (1992) Ablation of polymers and composites when exposed to CO₂ laser radiation (review). *Mech Compos Mater* 28:97–114. <https://doi.org/10.1007/BF00613315>
- Snakenborg D, Klank H, Kutter JP (2004) Microstructure fabrication with a CO₂ laser system. *J Micromech Microeng* 14:182–189. <https://doi.org/10.1088/0960-1317/14/2/003>
- Srinivasan R (1993) Ablation of polymethyl methacrylate films by pulsed (ns) ultraviolet and infrared (9.17 μm) lasers: a comparative study by ultrafast imaging. *J Appl Phys* 73:2743–2750. <https://doi.org/10.1063/1.353048>
- Steigert J, Haerberle S, Brenner T et al (2007) Rapid prototyping of microfluidic chips in COC. *J Micromech Microeng* 17:333–341. <https://doi.org/10.1088/0960-1317/17/2/020>
- Streets AM, Huang Y (2013) Chip in a lab: microfluidics for next generation life science research. *Biomicrofluidics*. <https://doi.org/10.1063/1.4789751>
- Strohmeier O, Keller M, Schwemmer F et al (2015) Centrifugal microfluidic platforms: advanced unit operations and applications. *Chem Soc Rev* 44:6187–6229. <https://doi.org/10.1039/C4CS00371C>
- Tang M, Wang G, Kong SK, Ho HP (2016) A review of biomedical centrifugal microfluidic platforms. *Micromachines*. <https://doi.org/10.3390/mi7020026>
- Tsao CW, DeVoe DL (2009) Bonding of thermoplastic polymer microfluidics. *Microfluid Nanofluidics* 6:1–16
- Urech L, Lippert T (2010) Photoablation of polymer materials. In: Allen NS (ed) *Photochemistry and photophysics of polymer materials*. Wiley, Hoboken, NJ, pp 541–568
- Włodkovic D, Darzynkiewicz Z (2011) Rise of the micromachines: microfluidics and the future of cytometry
- Zhu X, Liu G, Guo Y, Tian Y (2007) Study of PMMA thermal bonding. *Microsyst Technol* 13:403–407. <https://doi.org/10.1007/s00542-006-0224-x>

Publisher's Note Springer Nature remains neutral with regard to jurisdictional claims in published maps and institutional affiliations.